

# Synthesis and Photophysical and Photocatalytic Properties of a Highly Fluorinated and Durable Phthalocyanine–Peptide Bioconjugate for Potential Theranostic Applications

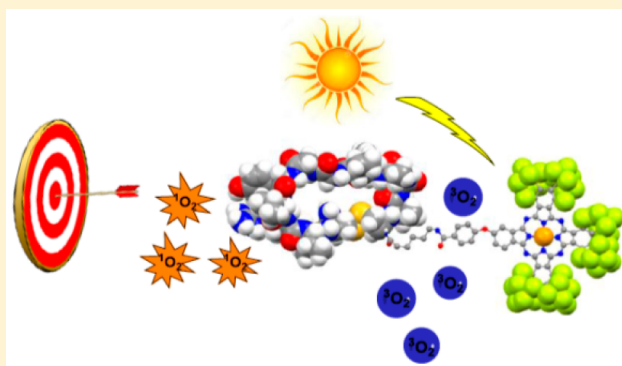
Erik N. Carrión,<sup>†,‡</sup> Jenyffer Santiago,<sup>†,‡</sup> David Sabatino,<sup>‡</sup> and Sergiu M. Gorun<sup>\*,†,‡,§</sup>

<sup>†</sup>Center for Functional Materials, Seton Hall University, 400 South Orange Avenue, South Orange, New Jersey 07079, United States

<sup>‡</sup>Department of Chemistry and Biochemistry, Seton Hall University, 400 South Orange Avenue, South Orange, New Jersey 07079, United States

## Supporting Information

**ABSTRACT:** The functionalized, asymmetric fluoro–fluoroalkyl scaffold  $F_{48}H_7COOHPcZn$  (**3**) was used to prepare  $F_{48}H_7COOPcZn$ -6-amino-hexanoate-CTVALPGGYVRVC (**5**), a Pep42 peptide bioconjugate envisioned for photodynamic therapy, which can specifically target the GRP78 chaperone protein overexpressed and exclusively localized on some cancer cell surfaces. The analogous  $F_{48}H_7COOHPcCu$  (**4**) has also been prepared, and its single-crystal X-ray structure was elucidated. Despite reduced steric hindrance relative to the nonfunctionalized, single-site complexes of the  $F_{64}Pc$  scaffold, no aggregation was detected in solution via UV–vis spectroscopy, for either **3**, **4**, or **5**, consistent with the lack of  $\pi$  stacking observed for the crystalline **4**. The 6-aminohexanoic acid-Pep42 moiety diminishes the fluorescence efficiency of **5**, relative to **3**, but for singlet oxygen ( $^1O_2$ ) generation, photochemical hydroperoxidation of  $\beta$ -(-)-citronellol using **5** and **3** occurs with comparable substrate turnover efficiency, albeit at a slower initial triplet oxygen uptake for **5**. The bioconjugate **5** is durable; it does not decompose under  $^1O_2$  photoreaction conditions. These results suggest a synthetic coupling pathway for obtaining diverse biotargeting polypeptide–fluorinated phthalocyanine bioconjugates of potential utility as both fluorescence reporters and photocatalysts and highlight the importance of fluorinated scaffolds for generating chemically resilient, catalytic, theranostic materials.



## INTRODUCTION

Theranostics combine therapeutic and diagnostic capabilities for accurate imaging and treatment applications.<sup>1</sup> Metal phthalocyanines (MPc's) are excellent candidates for theranostic applications because of their fluorescence, or phosphorescence, emission and the production of reactive oxygen species (ROS), such as singlet oxygen ( $^1O_2$ ), which can detect and kill malignant cells, respectively.<sup>2</sup> MPc's have several advantages over other photosensitizers, namely, (i) high molar extinction coefficients ( $\sim 100000\text{ M}^{-1}\text{cm}^{-1}$ ), (ii) high  $^1O_2$ /fluorescence quantum yields, (iii) near-IR (NIR) absorption (600–800 nm) for deep-tissue penetration, (iv) high thermal stability, (v) minimal dark toxicity, and (vi) tunable photophysical and photochemical properties by modifying peripheral or central atoms.<sup>3</sup> Closed-shell, central species, such as  $Zn^{2+}$ ,  $Al^{3+}$ , and  $Si^{4+}$ , are preferred in photodynamic therapy (PDT)<sup>4–6</sup> applications because of their “heavy atom effect” and diamagnetism that favor long triplet excited-state lifetimes, advantageous for efficient and long-lasting  $^1O_2$  production, provided that the phthalocyanine (Pc) is not degraded by the ROS it eventually produces.

Substituting the C–H bonds of the parent  $H_{16}PcZn$  with C–F bonds to give the  $F_{16}PcZn$  compound **1**, as shown in Figure 1, can favor a prolonged PDT effect by imparting Pc resistance to ROS.<sup>7</sup> However, the 16 aromatic C–F groups are susceptible to nucleophilic substitution, resulting in altered chemical, photophysical, and photochemical properties of the MPc's.<sup>8</sup> Moreover, the  $F_{16}Pc$  scaffold, unlike the parent  $H_{16}PcM$  scaffold, is prone to deactivating aggregation via  $\pi$ – $\pi$  stacking.

Consequently, a second-generation robust and sterically demanding perfluoroalkyl scaffold  $F_{64}Pc$  (**2**) has been designed (Figure 1). The design of the chemical robustness and steric hindrance exhibited by this scaffold is based upon eight perfluoroisopropyl groups located at the eight, more nucleophilic susceptible peripheral positions. They impart a 3D character to the parent, planar, 2D  $F_{16}Pc$  scaffold and thus improve the solubility in organic solvents. Their sterically bulky *iso* nature prevents  $\pi$ – $\pi$  stacking as well as nucleophilic attacks at the adjacent aromatic C–F groups. In addition, relative to  $F_{16}Pc$ , the eight perfluoroalkyl groups numerically halve the

Received: April 1, 2017

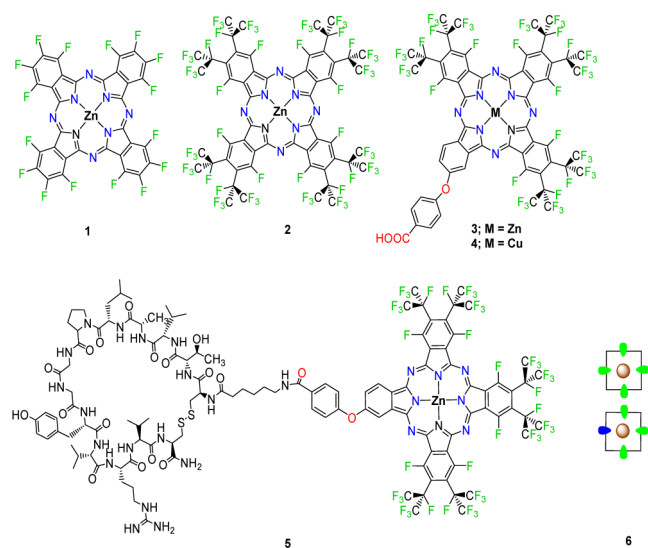


**Figure 1.** Logical progression of fluorophthalocyanine development. 1:  $F_{16}PcZn$  contains 16 coplanar aromatic C–F groups. In the parent  $H_{16}PcZn$  complex, all F atoms are replaced by H atoms. 2:  $F_{64}PcZn$  contains eight coplanar aromatic C–F groups and eight out of the molecular-plane, bulky perfluoroalkyl  $i-C_3F_7$  groups. 3 and 4: each contain six coplanar aromatic C–F groups and six bulky perfluoroalkyl  $i-C_3F_7$  groups, shown by the X-ray structure of 4 to be out of the molecular plane (Figure 2). The macrocycle is completed by a benzene ring containing three H atoms and one ether O atom at a peripheral position. A *p*-benzoic acid residue is linked to the ether O atom. 5:  $F_{48}H_7COOPcZn$ -6-aminohexanoate-Pep42. 6: schematic representation of the four quadrants of a Pc. Top: Symmetrical, 4-fold symmetry complexes of the type 1 and 2 with identical substituents in all four quadrants. Bottom: Asymmetrical complexes of the type 3–5 having only three quadrants bearing identical substituents.

degree of F back-bonding interactions while reducing, albeit to a lesser degree, the overall  $\sigma$ -withdrawing effects of the fluorine substituents. Overall, the metal centers become extremely Lewis acidic and thus are suitable for enhanced axial binding.

The zinc complex of the  $F_{64}Pc$  scaffold exhibits favorable photooxidation capabilities,<sup>9–11</sup> long triplet-state lifetime, and a high  $^1O_2$  quantum yield,<sup>11</sup> being a PDT photosensitizer capable of inducing 100% tumor regression in EMT-6 tumor bearing mice.<sup>9</sup> Both the first- and second-generation fluorophthalocyanines, however, given their largely nonspecific van der Waals interactions, forced by their fluorine substituents, exhibit poor specificity and thus potential toxicity because of their indiscriminate tissue dispersion.

Supplementing van der Waals interactions with potential covalent binding capabilities may allow the coupling of fluorophthalocyanines with a biovector that could impart tumor-homing abilities to the resulting bioconjugate. Bioconjugation of MPCs to tumor-homing ligands, such as oligonucleotides, peptides, and antibodies, can improve the PDT performance.<sup>12–16</sup> ZnPc's, Sonogashira-coupled to RGD and bombesin (Tyr-Gln-Arg-Leu-Gly-Asn-Gln-Trp-Ala-Val-Gly-His-Leu-Met-NH<sub>2</sub>) peptides, have been reported to exhibit cell uptake and photocytotoxicity by targeting integrin- and gastrin-releasing peptide receptors, respectively, in several tumor cell lines.<sup>17</sup> Trisulfonated ZnPc-bombesin produces phototoxic LD<sub>50</sub> values of  $<5 \text{ J cm}^{-2}$  in PC3, A549, MDA-MB-23, and EMT-6 cell lines. Similarly, tetrasulfonated ( $S_4$ ) AlPc, AlPcS<sub>4</sub>-bombesin conjugates exhibit a 2.5-fold increase in PDT activity against PC3 human prostate cancer cells relative to

AlPcS<sub>4</sub> alone.<sup>18</sup> A *t*-butyl-ZnPc-peptide conjugate targets the epidermal growth factor receptors (EGFRs) overexpressed on the cell surfaces of A431, Hep2, and HT-29 human carcinoma cells. Efficient fluorescence emission ( $\Phi_f = 0.10$ – $0.13$  at 680 nm) revealed an extended resident time within the EGFR overexpressing tumors.<sup>19</sup> The bulky *t*-butyl groups are sterically reminiscent of the fluoroalkyl groups of the  $F_{64}Pc$  and  $F_{48}Pc$  scaffolds, but they have opposite electronic effects, namely, releasing and withdrawing, respectively, while the C–H groups of the alkylphthalocyanine might be susceptible to ROS attack. The redox properties are also expected to be different, an aspect that may influence their *in vivo* stability and reactivity. On the other hand, both types of substituents are similarly enhancing the hydrophobic properties of the Pc's to which they are attached. Folic acid, coupled with asymmetric water-soluble PEGylated and glycerol-bearing ZnPc's, afforded significant Pc localization inside xenograft mice bearing malignant human epidermoid carcinoma, in the case of glycerolphthalocyanine for up to 7 h post-injection.<sup>20</sup>

Among chaperone proteins, GRP78 assists in protein-folding events in the lumen of the endoplasmic reticulum, regulating apoptotic executors, and maintaining  $Ca^{2+}$  flux in the mitochondria, while directing signal transduction at the cell surface.<sup>21</sup> In cancer, GRP78 is overexpressed and exclusively localized on the cell surface, thereby making it a therapeutically relevant biological marker for the development of GRP78-targeting ligands.<sup>22</sup> Pep42 (CTVALPGGYVRVC) is a hydrophobic peptide ligand, with selective GRP78-receptor-targeting capabilities,<sup>23</sup> discovered through phage display biopanning experiments. Pep42 has been used for the delivery of photosensitizers,<sup>23</sup> quantum dots,<sup>23</sup> and even Taxol<sup>24</sup> to carcinogenic melanoma cell lines in a GRP78-dependent manner. Pep42 has also been functionalized with polyarginine sequences, which enhanced cellular uptake relative to Pep42 in HepG2 cells, without causing any toxicity.<sup>25</sup>

Among partially fluorinated Pc conjugates, deoxyribonucleosides linked to trifluoroethoxy-substituted Pc's are noted, but they have been shown to exhibit oxidative instability.<sup>26</sup> Cyclodextrin-decorated trifluoroethoxy-substituted Pc's exhibit higher water solubility and PDT effects using a chicken embryo assay.<sup>27</sup> Galactopyranosylphthalocyanine conjugates exhibit water solubility, and the effect of Pc fluorination is viewed as beneficial for PDT activity via the induction of advantageous amphiphilicity.<sup>28</sup> Deoxyribonucleoside coupled to perfluoroalkyl-substituted Pc, prepared from our reported precursors,<sup>9</sup> confirmed the utility of the bulky perfluoroalkyl scaffold for preventing aggregation and enhancing chemical robustness, as demonstrated previously for 2. Good fluorescence quantum yields as well as improved stability under irradiation compared with trifluoroethoxy-substituted Pc's are noted. Notably, the fluoroalkyl-induced amphiphilicity is viewed as advantageous.<sup>29</sup>

We have recently reported that a carboxy-derived fluoroalkyl ZnPc,  $F_{48}H_7COOPcZn$  (3), was covalently attached to a linear antisense oligonucleotide that targets the GRP78 oncogene.<sup>16</sup> The MPC-oligonucleotide bioconjugate efficiently hybridized and photochemically oxidized oncogenic DNA and mRNA, making them susceptible to cleavage following a hot piperidine treatment.

Given the demonstration of the utility of peptide-derived MPCs in the treatment of tumors *in vitro* and *in vivo*, we sought to develop a heavily fluorinated PcZn-peptide bioconjugate using the potential GRP78 receptor targeting Pep42 (CTVALPGGYVRVC) hydrophobic peptide<sup>23</sup> but

exploiting the bioconjugate for both its PDT and fluorescence reporting abilities.

The target bioconjugate  $F_{48}H_7COOPcZn$ -6-amino-hexanoate-CTVALPGGYVRVC (**5**) and the logical progression of durable fluorophthalocyanine development from nonfunctional, van der Waals-type, first and second generations to functional **3** and covalently linked to peptide **5** are shown in Figure 1. Relevant molecular and solid-state structural information on the  $F_{48}H_7COOHPc$  scaffold was obtained via a single-crystal X-ray analysis of its copper(II) complex **4**.

## EXPERIMENTAL SECTION

Commercial reagents and solvents were used as received unless indicated otherwise. Perfluoro-4,5-diisopropylphthalonitrile and 4-(3,4)-dicyanophenoxybenzoic acid were prepared according to literature reports.<sup>30,31</sup> Pep42 (CTVALPGGYVRVC) was prepared according to the literature, using Fmoc solid-phase peptide synthesis on a NovaPEG Rink amide resin.<sup>23</sup>

**Synthesis.** The complex  $F_{48}H_7COOHPcZn$  (**3**) was obtained as described previously.<sup>16</sup> The complex  $F_{48}H_7COOHPcCu$  (**4**) was prepared by mixing perfluoro-4,5-diisopropylphthalonitrile (100 mg, 0.2 mmol), 4-(3,4)-dicyanophenoxybenzoic acid (52.8 mg, 0.2 mmol), copper(II) acetate monohydrate (19.9 mg, 0.1 mmol), and *n*-pentanol (20 drops) in a 10 mL Teflon-capped glass vial and heating to 200 °C for 15 min using a microwave CEM Discover reactor. The crude mixture was dissolved in ethyl acetate, extracted with  $H_2O$ , and chromatographed using  $SiO_2$ . Blue  $F_{64}PcCu$  was isolated in 15% yield, while **4** was isolated in 19% yield as a forest-green solid. <sup>19</sup>F NMR (376 MHz, acetone- $d_6$ ,  $CFCl_3$  std.):  $\delta$  71.51 ( $CF_3$ ), 101.32 (aromatic F), and 162.26 (tertiary F). The peaks are paramagnetically broadened and shifted relative to the diamagnetic **3**, whose corresponding resonances are observed at 71.35, 104.23, and 164.57 ppm, respectively.<sup>16</sup> ESI-MS. Calcd for  $C_{57}H_8F_{48}N_8O_3Cu$  (error: 4.8 ppm): 1826.9249. Obsd: 1826.9336. UV-vis [ $CHCl_3$ ;  $\lambda$ , nm ( $\log \epsilon$ ,  $M^{-1} cm^{-1}$ ): 711 (5.16), 673 (5.09), 607 (4.46), 362 (4.80)]. UV-vis [EtOH;  $\lambda$ , nm ( $\log \epsilon$ ,  $M^{-1} cm^{-1}$ ): 703 (5.08), 663 (5.04), 599 (4.40), 374 (4.74)]. In addition, adventitious  $Cl^-$  can bind to **4**, as evidenced by HRMS. Calcd for  $C_{57}H_8F_{48}N_8O_3CuCl^-$  (error: 5 ppm): 1861.89319. Obsd: 1861.90261. The 4-Cl ethanol (EtOH) mass spectrometry (MS) sample was spiked with 1% aqueous formic acid, resulting in the facile replacement of  $Cl^-$  by the  $HCOO^-$  anion, as demonstrated by HRMS. Calcd for  $C_{58}H_9F_{48}N_8O_5Cu$  (error: 8.8 ppm): 1871.92200. Obsd: 1871.93856. The isotopic patterns for  $[4-Cl]^-$  and  $[4-HCOO]^-$  are shown in Figure S1.

Complex **5** was synthesized by coupling **3** to resin-bound 6-amino-hexanoic acid (AHX)-Pep42 using 2-(6-chloro-1*H*-benzotriazole-1-yl)-1,1,3,3-tetramethylammonium hexafluorophosphate (HCTU) coupling conditions. Pep42 (CTVALPGGYVRVC) was prepared using Fmoc solid-phase peptide synthesis on a NovaPEG Rink amide resin.<sup>23</sup> Specifically, the N terminus of Pep42 was coupled to AHX prior to the bioconjugation reaction. **3** (23.75 mg, 0.013 mmol) and the resin-bound AHX-Pep42 sequence (25 mg, 0.013 mmol) were reacted with HCTU (5.35 mg, 0.013 mmol) and NMM (2.85  $\mu$ L, 0.026 mmol) in *N,N*-dimethylformamide (DMF; 1.5 mL) under continuous shaking for 16 h at 25 °C. The resin-bound bioconjugate was washed with 2  $\times$  15 mL DMF, methanol (MeOH), and dichloromethane to remove any unreacted **3** and excess coupling reagents, cleaved, and deprotected for 4 h using trifluoroacetic acid– $TES-H_2O$  (2.0 mL, 95:2.5:2.5, v/v/v). Filtration and precipitation with 3  $\times$  15 mL cold diethyl ether followed by centrifugation yielded **5** as a dark-green pellet (23% yield). Reverse-phase high-performance liquid chromatography (HPLC) analyses were performed using a Waters 2695 Alliance Separations Module with an Eclipse XDB C-18 column (4.6  $\times$  150 mm, 5  $\mu$ m particle size). Binary gradients of solvents A and B were employed at 1 mL  $min^{-1}$  flow rate, where A is 0.1% formic acid in Milli-Q  $H_2O$  and B is 0.1% formic acid in spectrophotometric-grade MeOH. A photodiode-array detector probed peptide and Pc presence at 220 and 680 nm, respectively.

UV-vis [EtOH;  $\lambda$ , nm ( $\log \epsilon$ ,  $M^{-1} cm^{-1}$ ): 702 (5.10), 664 (5.06), 382 (4.81)]. ESI-MS (Novatia, LLC). Calcd for  $C_{121}H_{112}F_{48}N_{26}O_{18}S_2Zn$  [error: 1.2 ppm, (M + H)<sup>+</sup>]: 3258.672. Obsd: 3258.668.

**Spectroscopy.** UV-vis–NIR spectra were obtained using a Varian Cary 500 spectrophotometer. Fluorescence emission spectra were recorded using a Horiba Jobin Yvon Fluorolog-3 (FL3-11) spectrofluorometer equipped with a 450 W xenon lamp with *FluorEssence v3.5* software. Fluorescence quantum yield calculations were performed using the comparative method,<sup>32</sup> with **3** as the experimental standard ( $\Phi_f = 0.07$  in EtOH) and calculated as follows:

$$\Phi_f^i = (F_f^i n_i^2 / F_f^s n_s^2) \Phi_f^s$$

where  $\Phi_f^i$  and  $\Phi_f^s$  are the fluorescence quantum yields of the sample and standard, respectively,  $F^i$  and  $F^s$  are the intensities of the sample and standard in units of photons,  $f_i$  and  $f_s$  are the absorption factors of the sample and standard at the excitation wavelengths ( $\lambda_{exc} = 615$  nm), and  $n_i^2$  and  $n_s^2$  are the refractive indices of the solvents for the sample and standard. Anhydrous EtOH was used for measurements of the MPC's. **3** was measured relative to  $F_{64}PcZn$  ( $\Phi_f = 0.15$  in EtOH), which was previously measured relative to literature-established  $H_{16}PcZn$  ( $\Phi_f = 0.20$  in DMSO).<sup>33</sup> Singlet excited-state lifetimes were measured using a time-correlated single-photon-counting technique. Samples were excited using a 671 nm NanoLED laser with a pulse width of <200 ps. The instrument response time was 22 ps (full width at half-maximum) determined with an aqueous colloidal silica suspension (Ludox) and setting the emission monochromator at the excitation wavelength, 671 nm. The sample concentration was adjusted to minimize inner filter effects. Lifetime data were processed using *DataStation v6* and were fit to a single-exponential decay with  $\chi^2 \sim 1.0$ . Circular dichroism (CD) spectra (molar ellipticity vs wavelength) of AHX-Pep42 and **5** in trifluoroethanol (50  $\mu$ M concentration) were measured using an Aviv 62A DS CD spectrophotometer. Three scans using 1 nm bandwidth and 0.5 nm step size from 190 to 260 nm at 25 °C were averaged, and the data were smoothed and converted to molar ellipticity using the equation  $[\theta] = \theta/d$ , where  $\theta$  is the relative ellipticity,  $c$  is the molar concentration, and  $l$  is the path length of the cell (10 mm). <sup>1</sup>H and <sup>19</sup>F NMR spectra were recorded at 25 °C using a Varian Inova 400 MHz instrument. <sup>1</sup>H and <sup>19</sup>F chemical shifts are referenced to the residual <sup>1</sup>H signal of  $CDCl_3$ ,  $\delta$  7.26, or the <sup>19</sup>F chemical shift of  $CFCl_3$ ,  $\delta$  0.00, respectively.

**X-ray Analysis and Molecular Modeling Studies.** Several single-crystal X-ray data sets were obtained for the weakly diffracting **4** using both Mo and Cu radiation. The results of the relatively best determination, using Cu radiation are reported. Molecular mechanics estimations of the bioconjugate **5** gas-phase architecture were obtained using *MOPAC2016*.<sup>34</sup> The computational approach was validated by a comparison between the calculated and observed X-ray structures of the  $F_{48}H_7COOHPc$  scaffold present in **3**–**5**. The two structures were virtually identical with the exception of the orientation of the benzoic acid moiety relative to the Pc ring, a variation most likely due to the free rotation around the single ether bonds and the intermolecular van der Waals packing interactions noted in the solid-state structure (see below) but absent in the gas-phase calculations.

**Catalysis.** <sup>1</sup>O<sub>2</sub> generation and in situ photohydroperoxidations of  $\beta$ -(-)-citronellol were performed at 25  $\pm$  0.2 °C under an O<sub>2</sub> atmosphere (99.998% purity) in a closed, 100 mL, thermostated, double-walled jacketed glass vessel. The reaction mixture consisted of 20  $\pm$  2  $\mu$ M photocatalyst dissolved in 50 mL of anhydrous EtOH containing 182  $\mu$ L (1.0 mmol) of  $\beta$ -(-)-citronellol. Illumination was performed using a 300 W halogen lamp with a light intensity of 2.8  $\pm$  0.1  $\times$  10<sup>5</sup> lux, measured at the outer wall of the reaction vessel with a light meter. O<sub>2</sub> consumption was monitored with a computer-interfaced Dosimat 665 (Metrohm, Herisau, Switzerland) gas titrator. The catalyst stability under the reaction conditions was monitored via UV-vis (300–800 nm) spectroscopy of 1 mL aliquots extracted periodically from the reaction mixture. Calibration was performed using **3** as the experimentally established standard with an oxygen

uptake of 27.8  $\mu\text{mol}$  of  $\text{O}_2 \text{ min}^{-1}$ .<sup>16</sup>  $^1\text{H}$  NMR was used to monitor the conversion of  $\beta$ -(-)-citronellol to its hydroperoxide regioisomers (Figure S2).<sup>35</sup> Gradients of acetonitrile/0.1 M phosphoric acid were utilized for the HPLC quantification of the hydroperoxides.

## RESULTS AND DISCUSSION

Complexes 1–3 and 5 are shown in Figure 1. 3 and 4 are isostructural except that 4 contains  $\text{Cu}^{\text{II}}$  instead of  $\text{Zn}^{\text{II}}$ . Complexes of the type  $\text{F}_{48}\text{H}_7\text{COOHPcM}$  [ $\text{M} = \text{Zn}$  (3), and  $\text{Cu}$  (4)] are the first representatives of the third-generation fluoroalkylphthalocyanines.

Considering that Pc macrocycles exhibit effective 4-fold coordination symmetry, the Pc aromatic rings can be viewed, formally, as composed of four quadrants. In the case of 2, as shown in Figure 1, each benzene ring quadrant exhibits two aromatic C–F groups and two out-of-the-molecular-plane, bulky  $i\text{-C}_3\text{F}_7$  perfluoroalkyl groups. These groups, as stated above, prevent intermolecular  $\pi$ – $\pi$  interactions and impart specific packing properties in the solid state. In the case of 3, only three quadrants exhibit antistacking bulkiness (Figure 1). The fourth quadrant bears the functional –COOH group. An ether group is located at a peripheral position, and thus a single isomer is obtained, a distinct advantage for structural, spectroscopic, and reactivity studies. However, stacking cannot be excluded a priori, and thus a potential lack of  $^1\text{O}_2$  production and PDT activity due to Pc excited-state lifetime shortening might occur.

The aggregation propensity of the  $\text{F}_{48}\text{H}_7\text{COOHPc}$  scaffold in the solid state was probed via single-crystal X-ray diffraction. Complex 3 yielded only poor-quality crystals despite numerous trials. The copper analogue 4 yielded slightly better crystals, which eventually allowed the determination of a structure of mediocre quality because of the large number of atoms (four molecules in the asymmetric unit), informative mainly regarding the connectivity, molecular conformation and stacking interactions, and overall packing (Figure S3). The copper(II) and zinc(II) structures of the  $\text{F}_n\text{Pc}$  scaffolds are very similar, as suggested by a comparison of the solid-state properties of  $\text{F}_{64}\text{PcZn}$  and  $\text{F}_{64}\text{PcCu}$ .<sup>9,36</sup>

The  $\text{F}_{48}\text{Pc}$  moiety of the organic scaffold, shown in Figure 2a, despite reduced intramolecular hindrance relative to the  $\text{F}_{64}\text{PcM}$  scaffold, where  $\text{M} = \text{Zn}$ ,  $\text{Co}$ ,  $\text{Cu}$ , and  $\text{V}=\text{O}$ ,<sup>9,36–38</sup> retains a similar architecture, namely, aromatic F groups almost in the plane of the macrocycle and  $\text{CF}_3$  groups, above and below this plane, defining a fluorinated pocket. The ether phenyl group that bears the –COOH group, site of covalent attachments, is twisted by about  $70^\circ$  away from the macrocyclic plane and extends, like an antenna, away from the  $\text{F}_{48}\text{Pc}$  scaffold (Figure 2b). MOPAC calculations of 5 in the gas phase yield the same geometry with the exception of the degree of rotation of the benzoic acid moiety, which, in the absence of solid-state packing forces, is now close to  $5^\circ$  (Figure S4).

Given the unhindered quadrant of the  $\text{F}_{48}\text{Pc}$  scaffold, one might anticipate head-to-tail-type intermolecular interactions, if any, in which the least bulky portion of the molecule, viz., the nonfluorinated benzene ring, is packed with the bulkiest one of another molecule, viz., the perfluoroalkyl groups of the opposite benzene ring. Figure 2c shows that dimers are indeed formed but in a head-to-head fashion, with the bulky  $i\text{-C}_3\text{F}_7$  perfluoroalkyl groups being in van der Waals contact. The Pc planes are parallel, but the intradimer interplanar distance is about 7 Å, too long for any meaningful  $\pi$ – $\pi$  interactions given that graphite, for example, exhibits 3.35 Å interplanar

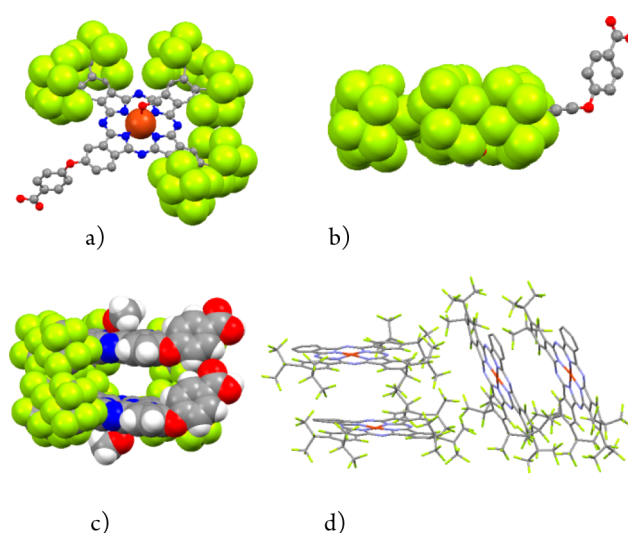


**Figure 2.** Molecular and solid-state structures of  $\text{F}_{48}\text{H}_7\text{-COOHPcCu-MeOH}$  (4-MeOH). Color code: Cu, orange; N, blue; O, red; C, gray; F, green; H, white. (a) Molecular structure of 4 depicting the Cu and F atoms using their van der Waals radii and the rest of the atoms as ball-and-stick. H atoms have been omitted for the sake of clarity. (b) 4 viewed along the Pc plane. (c) 4 dimer with all atoms depicted using their van der Waals radii. (d) Asymmetric unit showing the dimer of dimers. The  $p$ -benzoic acids and H atoms have been omitted for the sake of clarity. The remaining atoms are depicted as capped sticks.

separations. Similarly, the metal coordination number appears to be 5 based on MeOH axial coordination but could be 6 given that disordered MeOH molecules might be present in the space between the dimers (Figure 2c). Disordered, axial solvent coordination has been noted for  $\text{F}_{64}\text{PcZn}^{\text{II}}$ , whose metal exhibits no enthalpic ligand-field stabilization, but is also likely to occur for the isostructural  $\text{F}_{64}\text{PcCu}^{\text{II}}$ , which does but is likely subject to Jahn–Teller distortions and thus facile ligand exchange in solution. Indeed, spiking an EtOH solution of  $[\text{F}_{48}\text{H}_7\text{-COOHPcCuCl}]^-$  with 1% aqueous HCOOH resulted in a facile anion exchange that resulted in the formation of the complex  $[\text{F}_{48}\text{H}_7\text{-COOHPcCuHCOO}]^-$ . The dimer motif is retained throughout the structure; the four independent molecules present in the asymmetric unit appear as a dimer of dimers whose intradimer mean planes make a  $70^\circ$  angle (Figure 2d).

The X-ray-detected aggregation in the solid state prompted verification of aggregating properties in solution. The  $\text{F}_{48}\text{Pc}$  scaffold of 3 and 4 does not seem to aggregate.

A concentration-dependent UV–vis study in EtOH (Figure 3) was performed to determine whether any aggregation is observed spectroscopically for 5. Relative to 3, the bioconjugate 5 exhibits similar Q- and B-band absorptions, 382 (4.81), 664 (5.06), and 702 (5.10) for 5 versus 382 (4.81), 664 (5.02), and 702 (5.10) for 3.<sup>16</sup> Pc aggregation may be diagnosed using UV–vis spectroscopy by the appearance of blue-shifted bands ( $\sim 630$  nm), bands that increase or decrease at high/low concentrations, or broad Q bands ( $\sim 600$ – $850$  nm).<sup>39</sup> Such bands are not observed. The Beer–Lambert plots (Figure S5) are strictly linear, also indicating that no  $\pi$ – $\pi$  stacking occurs, because the van der Waals type aggregation observed in the solid state may not occur in solution and/or trigger a significant variation in the electronic structure of 5. The aggregation of 5 in the solid state could not be probed because crystals do not form. The lack of long-range ordering is consistent with

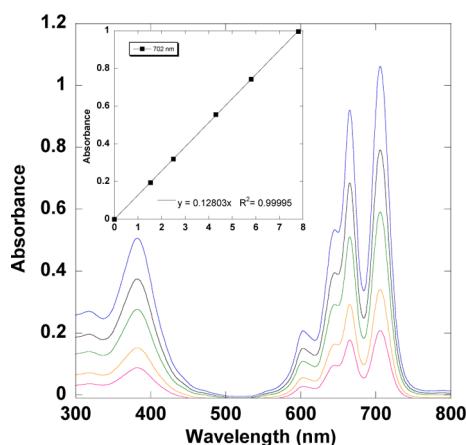


**Figure 3.** Concentration-dependent UV-vis absorption spectra of  $F_{48}H_7COOPcZn-AHX-Pep42$  in EtOH. Inset: Beer-Lambert plot at 702 nm. Additional plots at 382 and 664 nm are presented in Figure S5. A comparison in  $CHCl_3$  was precluded because of the insolubility of **4**.

difficulties in obtaining good-quality crystals even of unconjugated **3**.

The fluorescence emission spectrum (Figure S6), fluorescence quantum yields, and lifetime measurements of **5** were determined relative to **3**. The fluorescence quantum yield of **5** was 3.5-fold lower than that of **3** ( $\Phi_f = 0.02$  vs 0.07) but easily detectable. Both complexes exhibit a 12 nm Stokes shift. Fluorescence lifetime decay curves, fit to a single-exponential decay (Figures S7 and S8), revealed similar fluorescence excited lifetimes, 1.95–1.98 ns, but the radiative rate constant of **5** was  $1.01 \times 10^7 \text{ s}^{-1}$  versus  $3.58 \times 10^7 \text{ s}^{-1}$  for **3**. Given that the conjugation did not result in either a change in the UV-vis spectrum (Figure 3) or changes in Q- or B-band absorptions while the lifetimes of the excited states are similar, the diminished fluorescence yield might be due to static and/or dynamic quenching.<sup>40</sup>

Theranostic applications have a PDT component that could be advantageously implemented should the photosensitizer prove resistant to the  $^1O_2$  it produces. Complex **5** was thus tested for its ability to produce  $^1O_2$  in a sustainable manner.

Given that the premises for the lack of  $\pi$  stacking (single-site isolation) and invariability of the frontier orbitals of the  $F_{48}Pc$  scaffold after Pep42 conjugation have been met, the photochemical hydroperoxidation of  $\beta(-)$ -citronellol, a model photochemical reaction used for detecting  $^1O_2$  production with MPc catalysts, was employed.<sup>10</sup>  $\beta(-)$ -citronellol is a  $^1O_2$  trap. It reacts with  $^1O_2$  via Schenck-ene chemistry to generate a mixture of hydroperoxide regioisomers.<sup>35</sup>

The results of hydroperoxidation are shown in Figure 4. The  $\beta(-)$ -citronellol substrate is converted quantitatively to its hydroperoxides by **3** with an initial  $O_2$  uptake rate of  $27.8 \mu\text{mol of } O_2 \text{ min}^{-1} \text{ mol of Pc}^{-1}$  and a turnover frequency (TOF) of  $463 \text{ mmol of } \beta(-)\text{-citronellol s}^{-1} \text{ mol of Pc}^{-1}$ .<sup>16</sup> In comparison, **5** showed an initial  $O_2$  uptake rate of  $11.7 \mu\text{mol of } O_2 \text{ min}^{-1} \text{ mol of Pc}^{-1}$  and a TOF of  $196 \text{ mmol of } \beta(-)\text{-citronellol s}^{-1} \text{ mol of Pc}^{-1}$ . Importantly, in both cases,  $\beta(-)$ -citronellol is completely hydroperoxidized and the incorporated  $O_2$  represents the titrated  $O_2$ . In other words, 100% of the  $O_2$  released by the Dosimat is found in the hydroperoxide. The complete incorporation of  $O_2$  into the  $\beta(-)$ -citronellol-derived hydroperoxides was confirmed by  $^1H$  NMR and HPLC (Figures S2 and S9). The bioconjugate

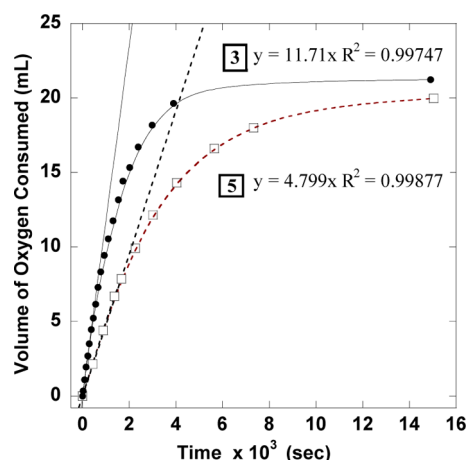


**Figure 4.** Photohydroperoxidation of  $\beta(-)$ -citronellol in EtOH using equimolar concentrations of **3** and **5** as catalysts. The time-dependent consumption of  $^3O_2$  was monitored with an automatic gas titrator. Hydroperoxide production was monitored via  $^1H$  NMR and HPLC. UV-vis was used to establish the stability of **3** or **5** during and after the reaction. See the text and Figures S2 and S9 for details.

catalyst **5**, like **3**, was found to be stable with no change in the UV-vis spectra before and after the photoreaction, for which the total oxidation number was set to 1000. Similarly, the paramagnetic **4** was also found to be both stable and active, albeit with a much lower TOF (data not shown).

The reasons for the lower TOF of **5** are not entirely clear, but the steric bulkiness of the tethered polypeptide, which occupies a space within the diffusion spheres of both  $^1O_2$  and  $\beta(-)$ -citronellol, as well as the changes in the local hydrophobicity imparted by the polypeptide may play a role. Although the initial rate of  $O_2$  uptake and the TOF of **5** are lower relative to those of **3**, the bioconjugate **5** remains an efficient and durable catalyst for the production of  $^1O_2$ .

Finally, the intramolecular steric effects of the conjugation were considered. MOPAC force-field calculations suggest that the Pc and peptide are spatially separated and thus unlikely to cross interfere with their functional roles, consistent with retention of the photocatalytic activity of **5**. CD studies are also congruent with the spatial and functional separation notion. Thus, as shown in Figure S10, the CD spectral comparison of AHX-Pep42 and **5** reveal key characteristic signals of an  $\alpha$ -helical structure of the peptide in both its Pc-conjugated and stand-alone forms.

PDT applications in vivo are traditionally viewed to require water solubility. Complex **5** is not water-soluble, but the even more hydrophobic, unconjugated **2** was used successfully for PDT studies in vivo by injecting it into mice as a cremophor preparation.<sup>9</sup> It has also been noted that perfluoroalkylation helps to balance the lipophilicity/hydrophilicity ratio of bioconjugates toward advantageous amphiphilicity.<sup>29</sup> Future PDT studies may provide more insight into the amphiphilic and other effects of heavy fluorination of bioconjugates.

In summary, the synthesis, photophysical, and photocatalytic properties of the first representative of the fluorophthalocyanine-targeting polypeptide class of bioconjugates  $F_{48}H_7COOPcZn-AHX-Pep42$  are reported. Solid-state studies revealed the lack of  $\pi$ - $\pi$  stacking of the  $F_{48}H_7COOPc$  scaffold, but van der Waals interactions led to dimers. UV-vis studies in EtOH revealed that  $F_{48}H_7COOPcZn-AHX-Pep42$  is monomeric in solution and does not form aggregates. Its

fluorescence, while diminished relative to the unconjugated **3**, is easily detectable, with the lifetimes of the excited state of poly-peptide, being invariable.  $^1\text{O}_2$  production, relevant for PDT applications, was confirmed using  $\beta(-)$ -citronellol, with the quantitative conversion of the substrate and full utilization of available  $\text{O}_2$  occurring without bioconjugate decomposition. The reactivity of **5** is consistent with the functional and spatial separation of the peptide from the Pc, as suggested by molecular mechanics calculations and CD demonstrating the retention of the  $\alpha$ -helical structure of the peptide upon conjugation.

In conclusion, the  $\text{F}_{48}\text{H}_7\text{COOPcZn-AHX-Pep42}$  bioconjugate provides an entry point into a new class of photoactive probes that may be useful in the rational design and development of robust catalytic drugs for theranostic and other PDT-based applications.

## ■ ASSOCIATED CONTENT

### ● Supporting Information

The Supporting Information is available free of charge on the ACS Publications website at DOI: 10.1021/acs.inorgchem.7b00847.

MS data,  $^1\text{H}$  NMR and HPLC of  $\beta(-)$ -citronellol and its hydroperoxides, X-ray information and ORTEP diagram for **4**, MOPAC calculations and Beer–Lambert plots for **5**, fluorescence emission spectra and lifetime measurements for **5**, and CD spectra of AHX-Pep42 and **5** (PDF)

### Accession Codes

CCDC 1548980 contains the supplementary crystallographic data for this paper. These data can be obtained free of charge via [www.ccdc.cam.ac.uk/data\\_request/cif](http://www.ccdc.cam.ac.uk/data_request/cif), or by emailing [data\\_request@ccdc.cam.ac.uk](mailto:data_request@ccdc.cam.ac.uk), or by contacting The Cambridge Crystallographic Data Centre, 12 Union Road, Cambridge CB2 1EZ, UK; fax: +44 1223 336033.

## ■ AUTHOR INFORMATION

### Corresponding Author

\*Tel.: 973-275-2133. E-mail: [sergiu.gorun@shu.edu](mailto:sergiu.gorun@shu.edu).

### ORCID

Sergiu M. Gorun: 0000-0003-1719-4086

### Author Contributions

The manuscript was written through contributions of all authors. All authors have given approval to the final version of the manuscript.

### Notes

The authors declare no competing financial interest.

## ■ ACKNOWLEDGMENTS

Financial support of the Center for Functional Materials, Seton Hall University, is gratefully acknowledged. The authors thank M. Phillips and N. Rana for providing a resin-bound peptide, W. R. Murphy for assistance in fluorescence data interpretation, and R. Lalancette and M. Neary for a portion of the X-ray data. R. Brukh is thanked for the MS data of **4**.

## ■ REFERENCES

- (1) Josefsen, L. B.; Boyle, R. W. Unique Diagnostic and Therapeutic Roles of Porphyrins and Phthalocyanines in Photodynamic Therapy, Imaging and Theranostics. *Theranostics* **2012**, *2*, 916–966.
- (2) Lau, J. T.; Lo, P. C.; Jiang, X. J.; Wang, Q.; Ng, D. K. A Dual Activatable Photosensitizer Toward Targeted Photodynamic Therapy. *J. Med. Chem.* **2014**, *57*, 4088–4097.
- (3) Ishii, K. Functional Singlet Oxygen Generators Based on Phthalocyanines. *Coord. Chem. Rev.* **2012**, *256*, 1556–1568.
- (4) Taratula, O.; Schumann, C.; Naleway, M. A.; Pang, A. J.; Chon, K. J.; Taratula, O. A Multifunctional Theranostic Platform Based on Phthalocyanine-Loaded Dendrimer for Image-Guided Drug Delivery and Photodynamic Therapy. *Mol. Pharmaceutics* **2013**, *10*, 3946–3958.
- (5) Chen, Z.; Zhou, S.; Chen, J.; Deng, Y.; Luo, Z.; Chen, H.; Hamblin, M. R.; Huang, M. Pentalysine-Carbonylphthalocyanine Zinc: An Effective Tumor-Targeting Photosensitizer for Photodynamic Therapy. *ChemMedChem* **2010**, *5*, 890–898.
- (6) Kyriazi, M.; Alexandratou, E.; Yova, D.; Rallis, M.; Trebst, T. Topical Photodynamic Therapy of Murine Non-Melanoma Skin Carcinomas with Aluminum Phthalocyanine Chloride and a Diode Laser: Pharmacokinetics, Tumor Response and Cosmetic Outcomes. *Photodermatol., Photoimmunol. Photomed.* **2008**, *24*, 87–94.
- (7) Allemann, E.; Rousseau, J.; Brasseur, N.; Kudrevich, S. V.; Lewis, K.; van Lier, J. E. Photodynamic Therapy of Tumours with Hexadecafluoro Zinc Phthalocyanine Formulated in PEG-Coated Poly(Lactic Acid) Nanoparticles. *Int. J. Cancer* **1996**, *66*, 821–824.
- (8) Leznoff, C. C.; Sosa-Sanchez, J. L. Polysubstituted Phthalocyanines by Nucleophilic Substitution Reactions on Hexadecafluorophthalocyanines. *Chem. Commun.* **2004**, 338–339.
- (9) Bench, B. A.; Beveridge, A.; Sharman, W. M.; Diebold, G. J.; van Lier, J. E.; Gorun, S. M. Introduction of Bulky Perfluoroalkyl Groups at the Periphery of Zinc Perfluorophthalocyanine: Chemical, Structural, Electronic, and Preliminary Photophysical and Biological Effects. *Angew. Chem., Int. Ed.* **2002**, *41*, 747–750.
- (10) Gerdes, R.; Lapok, L.; Tsaryova, O.; Wöhrl, D.; Gorun, S. M. Rational Design of a Reactive yet Stable Organic-Based Photocatalyst. *Dalton Trans.* **2009**, 1098–1100.
- (11) Beveridge, A. C.; Bench, B. A.; Gorun, S. M.; Diebold, G. Evaluation of Photodynamic Therapy Agents through Transient Grating Measurements. *J. Phys. Chem. A* **2003**, *107*, 5138–5143.
- (12) Duan, W.; Smith, K.; Savoie, H.; Greenman, J.; Boyle, R. W. Near IR Emitting Isothiocyanato-Substituted Fluorophores: Their Synthesis and Bioconjugation to Monoclonal Antibodies. *Org. Biomol. Chem.* **2005**, *3*, 2384–2386.
- (13) Master, A.; Malamas, A.; Solanki, R.; Clausen, D. M.; Eiseman, J. L.; Sen Gupta, A. A Cell-Targeted Photodynamic Nanomedicine Strategy for Head and Neck Cancers. *Mol. Pharmaceutics* **2013**, *10*, 1988–1997.
- (14) Ke, M.; Yeung, S.; Fong, W. P.; Ng, D. K. P.; Lo, P. A Phthalocyanine-Peptide Conjugate with High *In Vitro* Photodynamic Activity and Enhanced *In Vivo* Tumor-Retention Property. *Chem. - Eur. J.* **2012**, *18*, 4225–4233.
- (15) Nesterova, I. V.; Verdree, V. T.; Pakhomov, S.; Strickler, K. L.; Allen, M. W.; Hammer, R. P.; Soper, S. A. Metallo-Phthalocyanine Near-IR Fluorophores: Oligonucleotide Conjugates and Their Applications in PCR Assays. *Bioconjugate Chem.* **2007**, *18*, 2159–2168.
- (16) Patel, P.; Patel, H. H.; Borland, E.; Gorun, S. M.; Sabatino, D. Chemically Robust Fluoroalkyl Phthalocyanine-Oligonucleotide Bioconjugate and Their GRP78 Oncogene Photocleavage Activity. *Chem. Commun.* **2014**, *50*, 6309–6311.
- (17) Ranyuk, E.; Cauchon, N.; Klarskov, K.; Guérin, B.; van Lier, J. E. Phthalocyanine-Peptide Conjugates: Receptor-Targeting Bifunctional Agents for Imaging and Photodynamic Therapy. *J. Med. Chem.* **2013**, *56*, 1520–1534.
- (18) Dubuc, C.; Langlois, R.; Bénard, F.; Cauchon, N.; Klarskov, K.; Tone, P.; van Lier, J. E. Targeting Gastrin-Releasing Peptide Receptors of Prostate Cancer Cells for Photodynamic Therapy with a Phthalocyanine-Bombesin Conjugate. *Bioorg. Med. Chem. Lett.* **2008**, *18*, 2424–2427.
- (19) Ongarora, B. G.; Fontenot, K. R.; Hu, X.; Sehgal, I.; Satyanarayana-Jois, S. D.; Vicente, G. H. Phthalocyanine-Peptide Conjugates for Epidermal Growth Factor Receptor Targeting. *J. Med. Chem.* **2012**, *55*, 3725–3738.

- (20) Li, Y.; Wang, J.; Zhang, X.; Guo, W.; Li, F.; Yu, M.; Kong, X.; Wu, W.; Hong, Z. Highly Water-Soluble and Tumor Targeted Photosensitizers for Photodynamic Therapy. *Org. Biomol. Chem.* **2015**, *13*, 7681–7694.
- (21) Wang, M.; Wey, S.; Zhang, Y.; Ye, R.; Lee, A. S. Role of the Unfolded Protein Response Regulator GRP78/BiP in Development, Cancer, and Neurological Disorders. *Antioxid. Redox Signaling* **2009**, *11*, 2307–2316.
- (22) Wang, S.; Lee, A. C.; Chen, I.; Chang, N.; Wu, H.; Yu, H.; Chang, Y.; Lee, T.; Yu, J.; Yu, A. L.; Yu, J. Structure-Based Optimization of GRP78-Binding Peptides That Enhances Efficacy in Cancer Imaging and Therapy. *Biomaterials* **2016**, *94*, 31–44.
- (23) Liu, Y.; Steiniger, S. C. J.; Kim, Y.; Kaufmann, G. F.; Felding-Habermann, B.; Janda, K. D. Mechanistic Studies of a Peptidic GRP78 Ligand for Cancer Cell-Specific Drug Delivery. *Mol. Pharmaceutics* **2007**, *4*, 435–447.
- (24) Kim, Y.; Lillo, A. M.; Steiniger, S. C. J.; Liu, Y.; Ballatore, C.; Anichini, A.; Mortarini, R.; Kaufmann, G. F.; Zhou, B.; Felding-Habermann, B.; Janda, K. D. Targeting Heat Shock Proteins on Cancer Cells: Selection, Characterization, and Cell-Penetrating Properties of a Peptidic GRP78 Ligand. *Biochemistry* **2006**, *45*, 9434–9444.
- (25) Joseph, S. C.; Blackman, B. A.; Kelly, M. L.; Phillips, M.; Beaury, M. W.; Martinez, I.; Parronchi, C. J.; Bitsaktis, C.; Blake, A. D.; Sabatino, D. Synthesis, Characterization, and Biological Activity of Poly(Arginine)-Derived Cancer-Targeting Peptides in HepG2 Liver Cancer Cells. *J. Pept. Sci.* **2014**, *20*, 736–745.
- (26) Reddy, M. R.; Shibata, N.; Kondo, S.; Nakamura, S.; Toru, T. Design, Synthesis, and Spectroscopic investigation of Zinc Dodecakis-(trifluoroethoxy)phthalocyanines Conjugated with Deoxyribonucleosides. *Angew. Chem., Int. Ed.* **2006**, *45*, 8163–8166.
- (27) Obata, T.; Mori, S.; Suzuki, Y.; Kashiwagi, T.; Tokunaga, E.; Shibata, N.; Tanaka, M. Photodynamic Therapy Using Novel Zinc Phthalocyanine Derivatives and a Diode Laser for Superficial Tumors in Experimental Animals. *J. Cancer Ther.* **2015**, *6*, 53–61.
- (28) Mori, S.; Yoshiyama, H.; Tokunaga, E.; Iida, N.; Hayashi, M.; Obata, T.; Tanaka, M.; Shibata, N. Design, Synthesis, Spectral Investigations and Biological Activity of Fluorinated Phthalocyanine Conjugated with Galactose and Comparison to its non-fluorinated counterpart. *J. Fluorine Chem.* **2015**, *174*, 137–141.
- (29) Das, B.; Tokunaga, E.; Tanaka, M.; Sasaki, T.; Shibata, N. Perfluoroisopropyl Zinc Phthalocyanines Conjugated with Deoxyribonucleosides: Synthesis, Photophysical Properties and In Vitro Photodynamic Activities. *Eur. J. Org. Chem.* **2010**, *2010*, 2878–2884.
- (30) Gorun, S. M.; Bench, B. A.; Carpenter, G.; Beggs, M. W.; Mague, J. T.; Ensley, H. E. Synthesis and Structural Characterization of Non-Planar Perfluoro Phthalonitriles. *J. Fluorine Chem.* **1998**, *91*, 37–40.
- (31) Erdem, S. S.; Nesterova, I. V.; Soper, S. A.; Hammer, R. P. Mono-Amine Functionalized Phthalocyanines: Microwave-Assisted Solid-Phase Synthesis and Bioconjugation Strategies. *J. Org. Chem.* **2009**, *74*, 9280–9286.
- (32) Fery-Forgues, S.; Lavabre, D. Are Fluorescence Quantum Yields so Tricky to Measure? A Demonstration Using Familiar Stationary Products. *J. Chem. Educ.* **1999**, *76*, 1260–1264.
- (33) Li, Y.; Pritchett, T. M.; Huang, J.; Ke, M.; Shao, P.; Sun, W. Photophysics and Nonlinear Absorption of Peripheral-Substituted Zinc Phthalocyanines. *J. Phys. Chem. A* **2008**, *112*, 7200–7207.
- (34) MOPAC, version 17.068W; Stewart, J. P. Stewart Computational Chemistry, web site [HTTP://OpenMOPAC.net](http://OpenMOPAC.net), 2016.
- (35) Ohloff, G.; Klein, E.; Schenck, G. Darstellung von “Roseoxyden” und anderen Hydropyran-Derivaten über Photohydroperoxyde. *Angew. Chem.* **1961**, *73*, 578.
- (36) Moons, H.; Lapok, L.; Loas, A.; Van Doorslaer, S.; Gorun, S. M. Synthesis, X-ray Structure, Magnetic Resonance, and DFT Analysis of a Soluble Copper(II) Phthalocyanine Lacking C-H Bonds. *Inorg. Chem.* **2010**, *49*, 8779–8789.
- (37) Bench, B. A.; Brennessel, W. W.; Lee, H.; Gorun, S. M. Synthesis and Structure of a Biconcave Cobalt Perfluorophthalocyanine and its Catalysis of Novel Oxidative Carbon-Phosphorus Bonds Formation by Using Air. *Angew. Chem., Int. Ed.* **2002**, *41*, 750–754.
- (38) Lapok, L.; Lener, M.; Tsaryova, O.; Nagel, S.; Keil, C.; Gerdes, R.; Schlettwein, D.; Gorun, S. M. Structures and Redox Characteristics of Electron-Deficient Vanadyl Phthalocyanines. *Inorg. Chem.* **2011**, *50*, 4086–4091.
- (39) Howe, L.; Zhang, J. Z. Ultrafast Studies of Excited-State Dynamics of Phthalocyanine and Zinc Phthalocyanine Tetrasulfonate in Solution. *J. Phys. Chem. A* **1997**, *101*, 3207–3213.
- (40) Lakowicz, J. R. *Principles of Fluorescence Spectroscopy*; Springer: New York, 2006.